Photo-Induced Radicals in Carbon Nitride and their Magnetic Signature
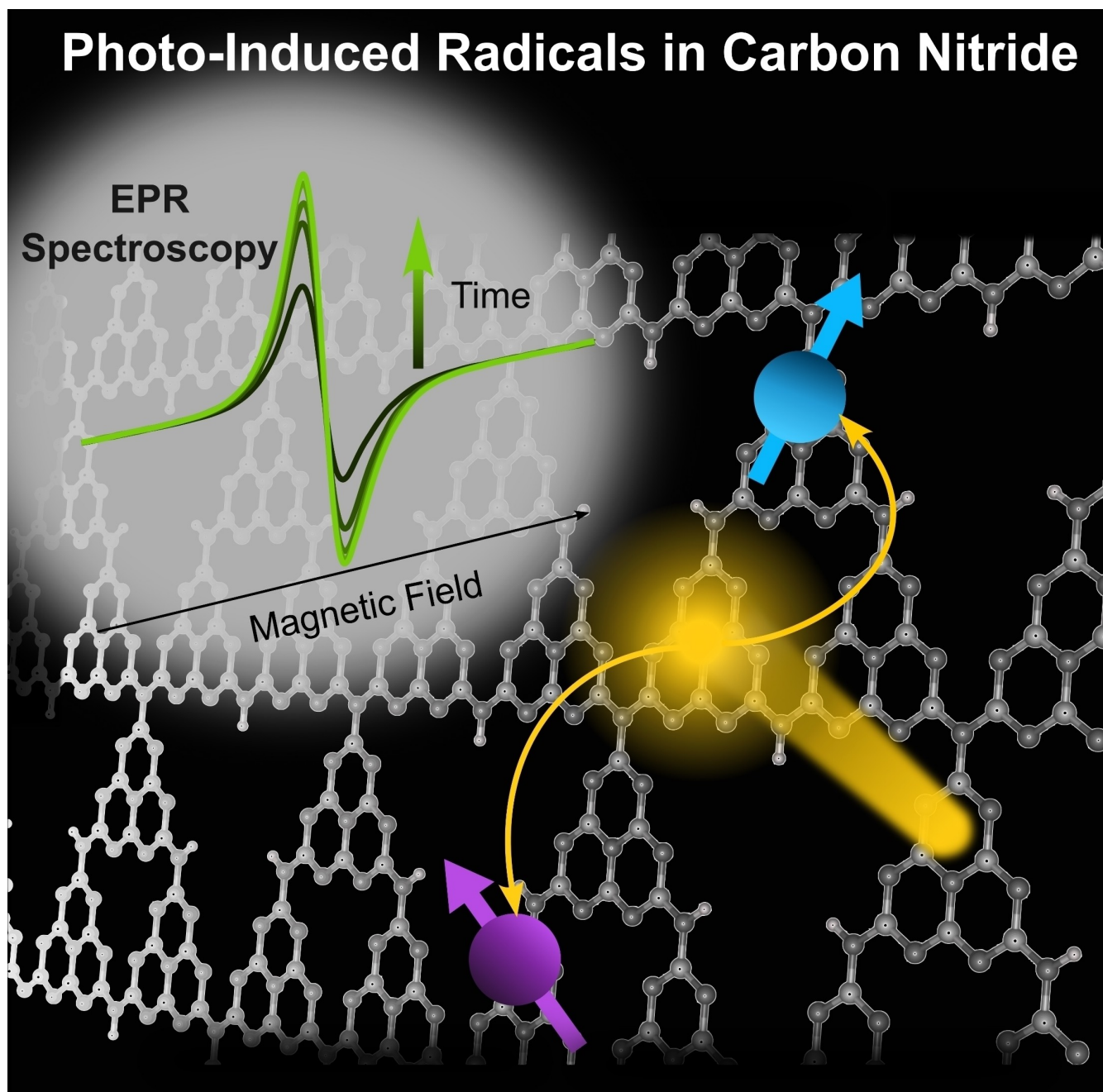
Arianna Actis,[a] Paolo Fornasiero,[b, c] Mario Chiesa,[a] and Enrico Salvadori*[a]

As a metal-free semiconductor, carbon nitride is a promising material for sustainable photocatalysis. From the large number of studies, it seems apparent that the photocatalytic activity is related to the number and type of defects present in the structure. Many defects are paramagnetic and photoresponsive and, for these reasons, Electron Paramagnetic Resonance (EPR) spectroscopy is a powerful method to derive fundamental information on the structure – local, extended and electronic – of such defects which in turn impact the optical, magnetic and chemical properties of a material. This review aims at critically discussing the interpretation of EPR data of native and photo-induced radical defects in carbon nitride research highlighting strengths and limitations of this spectroscopic technique.

1. Introduction

Carbon nitride (CN) is a generic umbrella term that includes a number of stoichiometries and structures. The most sought after is C_3N_4 which exists as several allotropes the most common of which are β-C_3N_4, analogue to diamond, and g-C_3N_4 (g-CN), analogue to graphite.[1]

g-CN is a non-specific term that comprises a rather broad family of materials, composed of graphitic layers and/or polymeric chains of N-rich aromatic rings. The monomeric units are constituted by 1,3,5-triazines[2] or tri-*s*-triazine (also known as heptazine) moieties linked by sp^3 hybridized N atoms.[3] The atomic C/N ratio in carbon nitride varies considerably, for instance for the ideal graphitic structure it corresponds to 0.75, whereas for the more realistic (and discussed) tri-s-triazine unit structure the theoretical C/N atomic ratio is 0.67, whereas the C/H atomic ratio corresponds to 2.0. CN contains only the earth-abundant elements carbon, nitrogen and hydrogen, can be synthetized from inexpensive and easily available precursors and has high chemical and thermal stability which is due to the strong covalent bonds between constituents in the conjugated layer structure. Because of the extensive conjugation, CN absorbs in the visible region of the electromagnetic spectrum with a bandgap of ≈ 2.7 eV ($= 460$ nm) and it has been successfully employed to catalyse a wide range of reactions. For all these reasons g-CN has quickly become a major player in current photocatalysis research.[4]

Despite all the appealing structural properties, the photo-catalytic activity of pure g-C_3N_4 is low due to its low absorption coefficient in the visible, and low specific surface area and efficient charge carriers recombination. To overcome these limitations defective structures have been engineered, by doping post or during growth with exogenous elements,[5] by exfoliation from bulk crystals,[6,7] by functionalising the edges of the layers with side groups[8,9] or by using high-temperature treatments[10,11] to increase the structural disorder and yield more amorphous materials (am-CN). Such modifications have proved effective in augmenting the efficiency and selectivity of CN towards specific (photo)chemical reactions.

Generally speaking, an effective photocatalyst, such as CN, must be able to accomplish a number of processes, which include: light harvesting, formation of excitons, separation into free charge carriers, charge transfer, and surface reactions[12]. Other events include: charge recombination, photolumines-cence and charge trapping in defective sites. Since most of the intermediates during a photocatalytic process possess unpaired electrons, Electron Paramagnetic Resonance (EPR) spectroscopy constitutes an excellent approach to investigate these steps. As it focuses on the magnetic properties, it is not hindered by the limitation of optical spectroscopy (e.g. light scattering, presence of overlapping signals, …) thus providing great selectivity and a complementary perspective to steady-state and transient optical spectroscopy. To highlight this complementarity, a summary of spectroscopic techniques, both optical and magnetic, used in CN research is reported in Figure 1 together with their scope and time resolution.

In this review we focus on the chemistry and physical properties of native and photoinduced radicals ($S = 1/2$) of carbon nitride, and particularly on current knowledge pertaining their local structure and to the mechanism by which light is captured and used to initiate photo-catalytic processes. The literature on carbon nitride is ever growing and EPR spectro-scopy is often used as a characterisation tool, the scope of this review is to guide the readers less familiar with the technique through the most easily encountered pitfalls in order to exploit this spectroscopy to its full potential. For this reason, we have carefully selected only a limited number of cases that are arguably most relevant to illustrate the technique. We wish to note that, although we discuss carefully chosen examples on specific morphologies and stoichiometries, the considerations we make and the guidelines we provide are general and applicable to whole CN materials.

[a] A. Actis, Prof. Dr. M. Chiesa, Prof. Dr. E. Salvadori
Department of Chemistry and NIS Centre, University of Torino, Via Pietro Giuria 7, 10125 Torino, Italy
E-mail: enrico.salvadori@unito.it
Homepage: https://www.chimica.unito.it/do/docenti.pl/Alias?enrico.salvadori#tab-profilo

[b] Prof. Dr. P. Fornasiero
Department of Chemical and Pharmaceutical, INSTM UdR, University of Trieste, Via Licio Giorgieri 1, 34127 Trieste, Italy

[c] Prof. Dr. P. Fornasiero
ICCOM-CNR URT Trieste, Via Licio Giorgieri 1, 34127 Trieste, Italy

2. Native and photo-generated spin defects

A schematic summary of the photophysical and photochemical processes responsible for the formation of photoinduced para-magnetic species in CN is reported in Figure 2. In detail, under photoexcitation of energy larger than the bandgap, ground state electrons in the valence band are promoted to the conduction band leaving, as a result, positive holes in the

ChemPhotoChem

Review
doi.org/10.1002/cptc.202300203

Chemistry Europe
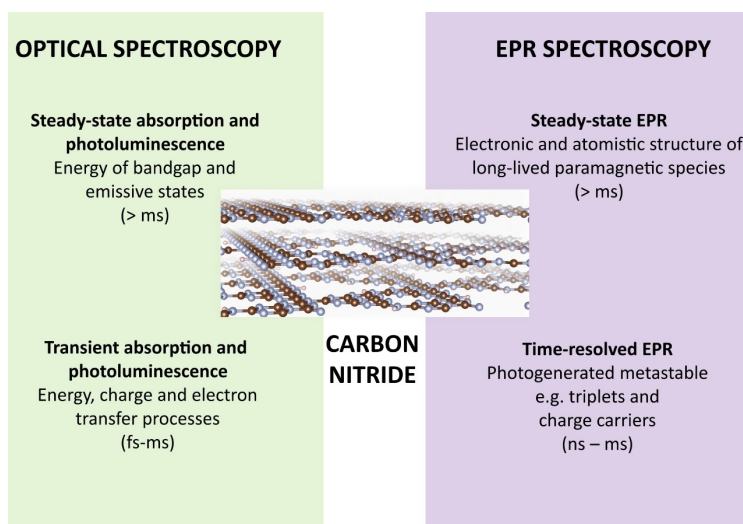European Chemical
Societies Publishing

Figure 1. Spectroscopic methods employed in CN photocatalytic research, their scope and relevant time resolution.

valence band. This process, which is spin-conserving, typically occurs on the femtoseconds time scale (10^{-15} s). Due to the low dielectric constant of carbon nitride, the electron/hole interaction is sufficiently strong to form a bound pair, also known as an exciton. Singlet excitons ($S = 0$), formed upon photoexcitation, may also evolve into triplet excitons ($S = 1$).[13] Recombination, which corresponds to the annihilation of the electron-hole pair, is a spin dependent mechanism that leads to the emission of a photon and relaxation to the ground state. Fast recombination processes are more likely to occur when the system retains the same total spin as the ground state, resulting in radiative (prompt photoluminescence) or non-radiative recombination (10^{-12}–10^{-7} s). On the other hand, excitons that change their spin state (singlet-triplet conversion), are more likely to result in long-lived states because the recombination to the ground state is spin forbidden. Their recombination, either radiative

(phosphorescence, delayed photoluminescence) or non-radiative, can occur on longer timescales (10^{-9}–10^{-3} s).[14] Excitons that do not recombine may diffuse within the material and eventually dissociate into free charge carriers ($S = 1/2$). The dissociation occurs if the energy difference between the donor and acceptor states is higher than the exciton binding energy, thus resulting in a net energy gain. These free carriers are central in photocatalysis as they have certain redox properties that can promote specific chemical reactivity, i.e. oxidation on the hole side and reduction on the electron side. It is to note that excitons and free charge carriers are intimately connected as the exciton binding energy is inversely proportional to the number of free carriers. Central to this discussion is also the presence of intra-bandgap states, which result from chemical defects within the regular structure of the material, that can promote exciton dissociation, serve as trapping sites for free

Arianna Actis is a Ph.D. student at the University of Torino under the supervision of Prof. Enrico Salvadori. Her research focusses on studying the photophysics and photochemistry of carbon nitride materials through magnetic resonance spectroscopy.

Mario Chiesa is Full Professor of Inorganic Chemistry at the University of Torino. His research interests are broadly based in the fundamental understanding of open-shell electronic structure, with applications ranging from catalysis to quantum information science.

Paolo Fornasiero is Full Professor of Inorganic Chemistry at the University of Trieste. His research interests are in the field of nanomaterial chemistry, with attention to their advanced applications in energy related material science and environmental heterogeneous catalysis.

Enrico Salvadori is Associate Professor of Inorganic Chemistry at the University of Torino. His current research efforts include the study of photoexcited paramagnetic states and the spatial distribution of defective species in solid-state inorganic materials.
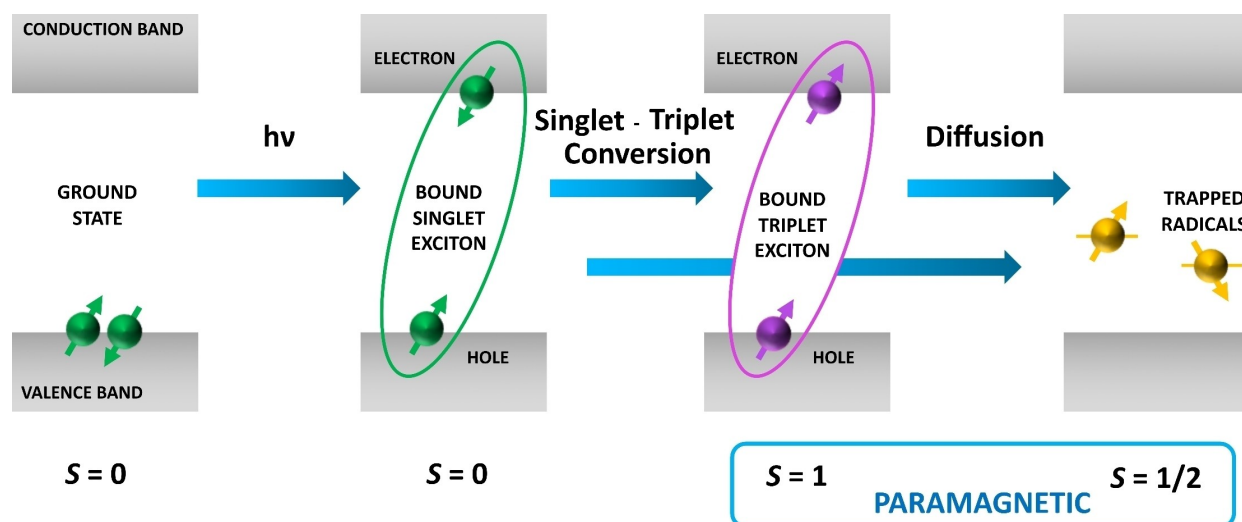
ChemPhotoChem

Review
doi.org/10.1002/cptc.202300203

Chemistry Europe
European Chemical
Societies Publishing

Figure 2. Schematic representation of the photophysical and photochemical processes leading to the formation of paramagnetic species after photoexcitation in carbon nitride (but applicable also to other semiconducting photocatalysts). The states amenable of EPR investigation are marked in blue.

charge carriers and are often important in dictating the photocatalytic activity of carbon nitride materials.

From a photochemical perspective, exploiting photophysical processes in CN to drive chemical reactions implies a thorough understanding of the fate of excitons and charge carriers, which is a non-trivial task in a poorly crystalline material such as CN. Electron/hole lifetimes can extend from fs to ms timescales, depending on the possibility of being stabilised at specific matrix sites which prevent their recombination. Native (structural) defects may on one hand enhance charge recombination processes, reducing the photocatalytic efficiency of the material or, on the other, may allow charges to survive long enough to migrate to the surface of the material and trigger photochemical transformations.

In the latter aspect, the spin state of the defect is fundamental in mediating electron transfers among the reagents. The role of the spin state is well known to drive structure-function relationships in metal complexes present in biological systems[15] and reactivity in homogeneous catalysis[16] and especially in organic chemistry, where reaction pathways involving singlet or triplet intermediates can be selectively addressed through molecular functionalisation.[17] This holds even more for photo-driven chemical conversions, where excited states with different spin may determine different chemo-, regio- and stereoselectivity.[18]

3. Electronic and defective structure of CN

One of the major challenges in the description of the electronic properties of real CN samples is due to its ill-defined structure and stoichiometry. This is because even within the same sample, chains of different length exist. Adopting here the semiconductor terminology as it is the most widely used in literature, this chemical and structural variability corresponds to intra bandgap states that are central in defining CN photo-

physics by creating low-lying absorption transitions and by acting as trap states for photogenerated charge carriers. A great deal of computational work has been done to rationalise the electronic and defective structure of CN, but there is no clear correspondence between the ideal theoretical model and the experimental data acquired on real samples.

EPR spectroscopy has been long and successfully employed to define the local structure of point defects in semiconductors[19] and is also often employed as a standard characterisation tool in CN research because photoirradiation often translates in an increased EPR signal, pointing towards a correlation between photoactivity and paramagnetic centres (Figure 3b). However, the extended π system of CN make the standard continuous-wave (CW) EPR signals almost featureless and difficult to interpret with atomistic detail. In the following sections we will try to illustrate the strength and limitations of EPR spectroscopy in this field of research. We will also introduce more advanced EPR techniques that, albeit less common, can provide a useful insight into the electronic and geometrical structures of defects.

4. EPR spectroscopy

EPR probes the interaction of the electron magnetic dipole moment with an applied magnetic field and electromagnetic radiation of the appropriate wavelength, usually in the microwave region of the electromagnetic spectrum.

For light-driven phenomena two main techniques can be employed: light-induced EPR (LEPR) and time-resolved (TR-EPR). The former can detect long-lived charge-carriers and trapped states by the "light on-light off" method, which consists in comparing the EPR spectra before, during and after light illumination. The latter directly detect the transient magnetisation generated after a light pulse and by virtue of a higher-time resolution of the order of 10–100 ns is suitable to detect
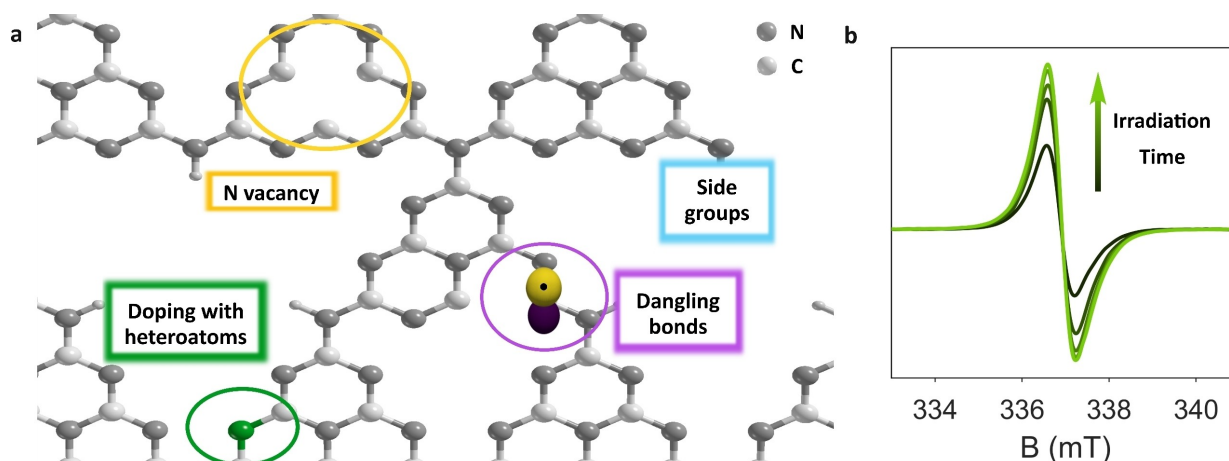
ChemPhotoChem

Review
doi.org/10.1002/cptc.202300203

Chemistry Europe
European Chemical
Societies Publishing

Figure 3. a) Schematic representation of the most common point defects present in CN. Structure derived from the Cambridge Structural Database, entry code: ICSD-194746[20] b) Representative CW EPR spectra of CN as a function of irradiation time. Data reproduced from ref.[11] Copyright (2021), with permission from Royal Society of Chemistry.a) provides a pictorial description of the most common paramagnetic defects discussed in the literature, which include N and C vacancies (i.e. sub-stoichiometry), disruption of the conjugated system to form dangling bonds, chemical substitution by heteroatoms and the presence of side groups. We wish to point out that defects can in principle exist as empty, doubly and singly occupied. While they are all relevant in defining the physical and chemical properties of the material, only singly occupied (i.e. paramagnetic) defects can be addressed by EPR spectroscopy.

metastable photo-excited states such as triplets as well as charge carriers.

An EPR spectrum is usually characterised by the position of the resonance line (i.e. interaction between the electron spin and the applied magnetic field) and by hyperfine splitting(s) due to the surrounding magnetic nuclei. A concise and operative introduction to these interactions is provided in the following. The readers interested in a more in-depth discussion are referred to.[21,22,23]

4.1. The g-factor

The g-factor quantifies the interaction between the magnetic moment of the unpaired electron and the applied magnetic field, is akin to the chemical shift used in NMR and, in favourable cases, serves as an identifier for a given paramagnetic species.

The magnetic moment of a free-electron in vacuum, $\boldsymbol{\mu}$, is proportional to the electron spin angular momentum ($\boldsymbol{S} = 1/2$) according to the relationship: $\boldsymbol{\mu} = -g_e\beta_e\boldsymbol{S}$ (in unit of $\hbar$), where $\hbar$ is the reduced Planck's constant and β_e is the Bohr magneton. g_e, called the g-factor of the free electron, is a physical constant known with extraordinary precision ($g_e = 2.0023318416(13)$).

In real systems unpaired electrons are not isolated charges in vacuum, but are confined in atomic or molecular orbitals defined by the surrounding nuclei and their connectivity, therefore their g-value deviates from g_e depending on the chemical environment ($\Delta g = g - g_e$). Generally speaking, in solids, g is not a scalar but a 2nd-rank tensor which reflects the ground-state symmetry of the paramagnetic specie. The average of the principal components of the g-tensor is known as the isotropic g-factor, g_{iso}.

Understanding the factors influencing the measured g-value of a specific signal are fundamental to a proper interpretation

of EPR data and to derive meaningful information on the electron structure of paramagnetic defects, especially for the typical (featureless) EPR spectra observed for CN.

The main reason for the deviation from g_e is due to the spin-orbit interaction which couples the spin angular momentum ($\boldsymbol{S}$) with the orbital angular momentum ($\boldsymbol{L}$), which is usually quenched in molecular systems. The strength of the coupling, and hence the deviation of the measured g-value from g_e, depend on the spin-orbit coupling constant and the energy difference between the ground and excited states. As an example, organic radicals where the unpaired electron is mainly localised in carbon p_π orbitals generally have small Δg, since the spin orbit coupling constant for C is small and the excited states are very high in -energy. For this reason, when dealing with paramagnetic defects centered on light elements, such as carbon and nitrogen, great care should be exerted in determining the experimental g-factor to draw meaningful conclusions. For reference, Table 1 reports a collection of g-factors measured for carbon-centered radicals in solid-state systems. It can be clearly seen that different species can only be reliably determined by comparing the fourth decimal digit.

In general, it is possible to outline some rules to help interpret the g-values of carbon-cantered radicals similar to

Table 1. Literature data for carbon-centered solid-state inorganic systems. For each species a range of literature values is provided.

Species	g factor(s)	Ref
Amorphous carbon Csp^2	2.0028–2.0030	24 25
Amorphous carbon	2.0022–2.0031	26 27 28 29 30
Bulk and exfoliated graphite	2.003	31
Graphene oxide (GO)	2.00278–2.00288	32 33
GO, near O-groups	2.0031	34

ChemPhotoChem

Review
doi.org/10.1002/cptc.202300203

Chemistry Europe
European Chemical
Societies Publishing

those expected in CN, for ease of comparison we restrict to the isotropic g-value:

- Purely carbon-centered radicals (e.g. methyl and ethyl) have $g = 2.0026 \pm 0.0001$
- the g-factor of σ radicals, is usually lower than for their π counterparts
- Radical anions exhibit distinctively larger g-factor than the corresponding radical cations
- Introduction of a heteroatom into a π radical generally increases the g-factor, the heavier the heteroatom the larger the shift

A collection of characteristic g-factors, that summarize the rules outlined above, is reported in Table 2.

4.2. Measuring the g-value

In the presence of an applied magnetic field (B_0), the energy separation between spin sublevel ($m_S = \pm \frac{1}{2}$) is given by $\Delta E = \hbar\omega = g\beta_e B_0$. Given that g is a constant, the relationship implies that the splitting increases as the strength of the applied magnetic field increases.

In order to discriminate amongst the different paramagnetic species present in a sample, the g value must be determined with a sufficient precision and with enough decimal digits. The major source of uncertainty in the determination of the g value arises from the magnetic field. In most commonly used EPR spectrometers the magnetic field is measured through a Hall probe, which however is not at the sample space. This results in an offset between the actual field experienced by the sample and the measured one. The most common procedure to calibrate the offset is by means of a standard sample with known g value (ex. solid DPPH)[37]. In order to discriminate different paramagnetic species in organic radicals (i.e. C-based radicals), the determination of the g value should reach at least the fourth decimal digit. A considerable increase in resolution can be achieved by working at higher microwave frequency, as in the example reported in Figure 4 that compares experimental EPR spectra recorded for a sample of CN in dark and under VIS illumination at two microwave frequencies (9 and 34 GHz).[38,39] As shown, increasing the working microwave frequency not only allows to (partially) resolve the components of the g-matrix (the black spectrum at 34 GHz is less symmetric than the
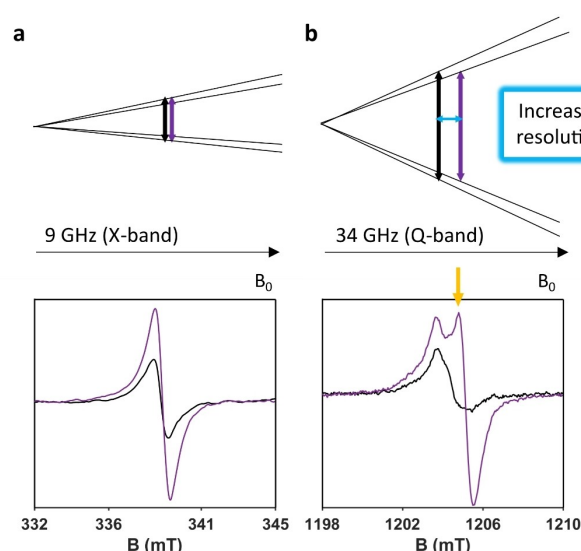

Figure 4. a) schematic representation of two spin with similar g values at 9 GHz (top) and (bottom) the corresponding experimental EPR spectrum in dark (black) and under VIS illumination (purple). b) schematic representation of two spin with similar g values at 34 GHz (top) and (bottom) the corresponding experimental EPR spectrum in dark (black) and under VIS (500 nm for Q band) illumination (purple). The increased resolution is marked by the blue arrow. The radical species formed only under illumination is marked by the yellow arrow. Data reproduced from ref.[39] Copyright (2023), with permission from Wiley-VCH.

counterpart at 9 GHz), but also permits to ascertain the formation of a new spin species formed only under photo-excitation.

Given the extremely high variability of structure and composition displayed by CN - which depend on the precursors used, the elemental composition and the synthetic and post-synthetic treatments applied - caution should be exerted when comparing EPR studies (and spectroscopic studies in general) on CN.

From a survey of the literature, we can conclude that most of the EPR data reported in literature are collected at 9 GHz (X-band) and exhibit a CW EPR spectrum constituted by a nearly isotropic signal, with g-factor falling in the range ∼2.003-2.004. This signal is usually detectable even prior to photoexcitation (dark) and is attributed to radical defects intrinsically present in the sample. This characteristic signal has been ascribed to localised unpaired electrons hosted in the p orbital belonging to a sp^2 hybridised C atom. Several studies observed an increase in the radical signal intensity as the N content in the material decreased and suggested a correlation between the two suggesting the formation of nitrogen vacancies.[40,41,42]

Table 3 collects the most accurate g values for CN, either because collected at high microwave frequency or measured on well oriented samples. They refer to different morphologies and to materials prepared through different procedures, but serve to illustrate the typical values and the spread that may be expected from an EPR measurement.

Despite the different synthesis procedures and final physical and optical properties of CN materials, the g factors reported appear quite consistent.[43,46] The positive g shift with respect to

Table 2. Isotropic g factors of various classes of carbon-centred radicals.	
Type of radical	Isotropic g-factor
Alkyl radicals[35]	2.0026
Vinyl[35]	2.0022
Phenyl[35]	2.0023
Poly-acenes radical anions[36]	2.002667–2.003067
Poly-acenes radical cations[36]	2.002565–2.002605
Azaaromatics[35]	2.0030–2.0035
Oxo-substituted[35]	2.0040–2.0060
S-containing compounds[35]	2.0070–2.0080

ChemPhotoChem

Review

doi.org/10.1002/cptc.202300203

Chemistry Europe
European Chemical
Societies Publishing

Table 3. *g*-factors for CN species.

Material	*g*-factor	Notes	Reference
am-CN	2.0042	Q-band	39
g-CN	2.0037–2.0051	Q-band, multiple species	39
gC$_x$N$_y$H$_z$	2.0034–2.0035	X-band, rotation pattern	43
Carbon-nitrogen network	2.0032	139.5 GHz	44
NCN-CN$_x$	2.00275	W-band (94.2 GHz)	45

g_e is in line with the elemental composition of CN, which alternates C and N atoms in the structure.[47] Beside the general agreement among the reported *g* values, higher variability can be found in the signal line shape. Measurements conducted on bulk or thin film CN can either yield a homogeneously broadened Lorentzian signal[46,48,49] or a heterogeneously broadened Gaussian line shape attributable to unresolved hyperfine couplings.[43] This reflects the high variability which affects the final structural properties of this material as a consequence of the different synthetic processes but may also, at least partially, depend on the experimental conditions employed which should also be clearly specified. The dark EPR signal almost invariably increases under visible light illumination, suggesting a redistribution of electrons within the material.[11,50,51] Some papers[48,52] have attributed this light-dependent EPR signal to conduction electrons. However, electrons occupying the conduction band should be very delocalised within the material displaying a characteristic temperature dependence (Pauli's paramagnetism) and a lineshape that depends on the particle size and the conductivity of the material.[21,53] In CN there is no report of such specific lineshape, this is in line with the poor electron conduction properties displayed by this material, which derive from the electronically isolated tri-s-triazine or triazine within the scaffold.[54]

4.3. Quantifying the number of spins

CW EPR spectra can be used to determine the absolute number of spins (or their concentration) present in a sample. The assumption is that each spin behaves independently (weak coupling as compared to the distribution of Larmor frequencies) and therefore that the double integral of the signal is linearly proportional to their number. Furthermore, if the unpaired electrons couple to a well-defined spin S > 1/2, it is still possible to conduct quantitative EPR, provided that S is considered in the analysis. For a proper spin quantification, CW EPR spectra must be acquired with a microwave power which does not distort (i.e. saturate) the EPR transition. This means that the microwave power must be chosen within the range of linear dependence of the signal intensity from the square root of the power ($I \propto \sqrt{P}$). Once acquired the experimental spectrum (first derivative) and performed a baseline correction to avoid artefacts, an experimental calibration with samples of known

concentrations allows to correlate the double integral to the absolute number of spins in the sample. If the mass and volume of the sample are known, the overall spin concentration can be obtained. More recently, some commercial EPR programs permit to achieve the same result without the need of standard samples. To minimise error, when possible, standard samples should be of the same concentration and chemical type as well as physical phase and volume. Several factors which can also affect the measurement must be taken into consideration, especially when comparing spin counting on different samples. These include the position of the sample in the resonator due to the magnetic field inhomogeneity (affecting the resonance condition of the spins), the temperature (acting on the Boltzmann population of the spin states and, therefore, on the signal intensity), and many other parameters strictly related to the specific spectrometer.[37] When dealing with native and photogenerated paramagnetic species in carbon nitride it is fundamental to take all these factors into account (and provide them in the experimental section) in order to provide meaningful and reproducible results.

4.4. Hyperfine interaction

The most chemically useful information derivable from an EPR spectrum is encoded in the hyperfine coupling between the unpaired electron and the magnetic moments of neighbouring magnetic nuclei. Hyperfine coupling usually enables identification of the radical and also the detailed assessment of its electronic and geometric structures. The hyperfine interaction manifests as a splitting of the EPR line, for instance *n* equivalent nuclei of spin *I* result in $(2nI+1)$ lines and the separation between each of these lines is (to first-order) equal to the hyperfine splitting constant. If more classes of magnetically active nuclei are present, the total number of lines is given by $\prod_1^k (2n_k I_k + 1)$, where n_k is the number of equivalent nuclei and I_k is the respective nuclear spin quantum number. This easily leads to a complex or even unstructured EPR signal as the number of coupled nuclei increases. Analysis of the hyperfine interaction yields detailed information on the chemical environment and the nature of the chemical bonds. For nuclei at distances > 2.5 Å the hyperfine interaction can be expressed in the point-dipole approximation as:

$$T = \frac{\mu_0}{4\pi\hbar} g\beta_e g_N \beta_N \frac{3\cos^2\theta - 1}{\langle r^3 \rangle} \tag{2}$$

where θ is the angle between the vector joining electron and nuclear spin moments and the applied magnetic field, whereas *r* is the electron-nuclear distance. Hence, it allows to measure the electron-nuclear distances.

Large hyperfine couplings (> 0.2 mT) can be directly determined by CW EPR spectroscopy whereas small hyperfine couplings are best retrieved by the use of pulsed methods such as ENDOR (Electron-Nuclear DOuble Resonance) and HYSCORE (HYperfine Sublevel CORrElation spectroscopy). Given the technical detail needed for a proper introduction to these

ChemPhotoChem

Review
doi.org/10.1002/cptc.202300203

**Chemistry
Europe**
European Chemical
Societies Publishing

techniques the interested reader is referred to recent reviews on the topic[55,56]. We only note that the structural details affordable by hyperfine techniques can compete with X-ray-based and NMR-based structural characterization methods.[57–59]

Since ^{12}C has no magnetic moment, proton (^1H, $I = 1/2$) and nitrogen (^{14}N, $I = 1$) hyperfine couplings should dominate the EPR spectra. However, no such couplings are readily detectable in a CW EPR experiment suggesting that the unpaired electron is fairly delocalised over the CN structure. In turn this suggests that the radical species observed in CN are π-radicals.[11,38,39,44] More sophisticated pulsed EPR techniques (e.g. ENDOR and HYSCORE) were able to retrieve this information.[39,45] Figure 5 reports the ENDOR and HYSCORE spectra for amorphous CN. ENDOR yields a ^1H hyperfine coupling (**T** in Eq 2) of 0.7 MHz which corresponds to an electron-nucleus distance of about 4.3 Å,[39] whereas HYSCORE provides for ^{14}N an a_{iso} of 0.9 MHz and a dipolar component of 0.8 MHz as well as a nuclear quadrupole coupling $e^2qQ/h = 3.0$ MHz.[39,60] Such a small hyperfine coupling for ^{14}N stems from a high degree of electron delocalisation and justifies the absence of any discernible splitting in CW EPR. The average radical - ^1H distance of ∼4.3 Å compares well with the distance between the centre of a tri-s-triazine unit and the edge of such structural motif in the crystal structures considered.[20] This, together with the small ^{14}N hyperfine coupling, further suggests that the radical species is delocalised but likely confined on a tri-s-triazine unit.

Hyperfine techniques were also applied by Lotsch et al. to obtain a fine description of the structural and optical behaviour of photo-induced species of a specific CN material based on a polyheptazine imide, but subject to a post-synthetic ionothermal treatment with KSCN to introduce cyanamide functionalities as terminating groups.[45] Combination of ^{14}N HYSCORE with computational modelling allowed to identify charge-neutral cyanamide group as traps for photo-excited electrons, demonstrating how EPR techniques serve as a formidable tool to assess defect-engineering.

Given the high degree of delocalisation caution should be exerted when interpreting hyperfine data of conjugated solids like CN without knowledge of the wavefunction. This is because the hyperfine interaction depends on the wavefunction which, in the case of π systems, does not decay monotonically with distance and exhibit maxima and minima at specific nuclei.

4.5. Computational chemistry on CN

As demonstrated by the previous examples, unfortunately the EPR constraints alone do not suffice to provide an atomistic structural description of defects in CN and quantum-chemical methods computations are needed to suggest viable structure. The computed spectroscopic properties can then be scored, validated or rejected on the basis of the EPR experimental results. An example of this procedure was proposed by Lazzaroni et al.[60] Starting from graphitic CN structure, the hypothetical defect-free heptazine-based CN structure, the authors computed the formation energies of possible defective sites. Such structural modifications were chosen based on post-synthetic experimental treatment (i.e. thermal, reduction or oxidation processes conducted on the as-synthesised graphitic CN[61] and previous computational models.[62,63] For instance, nitrogen losses were experimentally observed when graphitic CN undergoes thermal ("amorphization") treatments, therefore structural models with nitrogen vacancies were computed and their electronic structure and stability were evaluated. In general, given that CN has a rich structural variability and can only be prepared as a polycrystalline material lacking long range order, computational results must be considered with caution and only as *possible* solutions.[8,9]

4.6. Spatial distribution of native and photoinduced radical defects

A recent addition to the toolbox offered by EPR is constituted by the family of pulsed dipolar spectroscopy (PDS) techniques, which exploit the magnetic dipole-dipole interaction between pairs of weakly-coupled electron spins (i.e. two $S = 1/2$) to measure nanometre-scale distances.[64,65] The use of PDS spectroscopy constitutes a powerful methodology to derive the long-range spatial distribution (nanometer) of paramagnetic species in solid-state materials[66] with high precision which complements for the local (sub-nanometer) structural detail obtained through hyperfine spectroscopy. The measured inter-spin distance can then be compared with the available X-ray structure to determine the most likely spatial location of pairs of radicals. Application of such technique at 34 GHz allowed to derive the spatial distribution of native and photoinduced radical defects in CN. This yields a nearest-neighbour distance in the range 1.99–2.34 nm, which corresponds to pairs of radical species located four tri-s-triazine units away.

Furthermore, even though light irradiation results in a higher concentration of radical defects their nearest-neighbour distance does not change indicating that intra bandgap states are far from being saturated and are well isolated and sparsely populated. This is also supported by the comparison of the radical concentration and the number of tri-s-triazine units, which allows to estimate 1 radical every 10^5 units.
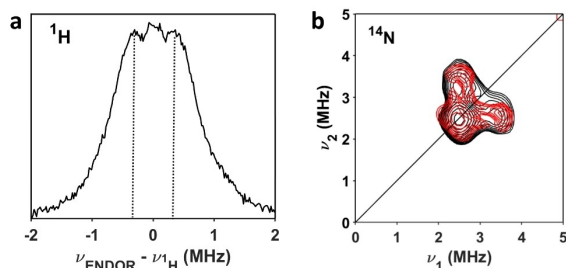

Figure 5. a) Representative ^1H Mims ENDOR spectrum of CN. The frequency scale on the x-axis reports the deviation of the resonance line from the Larmor frequency (ν_H) recorded at 50 K and at 1204.75 mT. Data adapted from ref.[39] Copyright (2022), with permission from Wiley-VCH. b) Representantive ^{14}N HYSCORE spectrum of CN (black) and corresponding simulation (red) with parameters reported in the text. Data adapted from ref.[60] Copyright (2023), with permission from Royal Society of Chemistry.
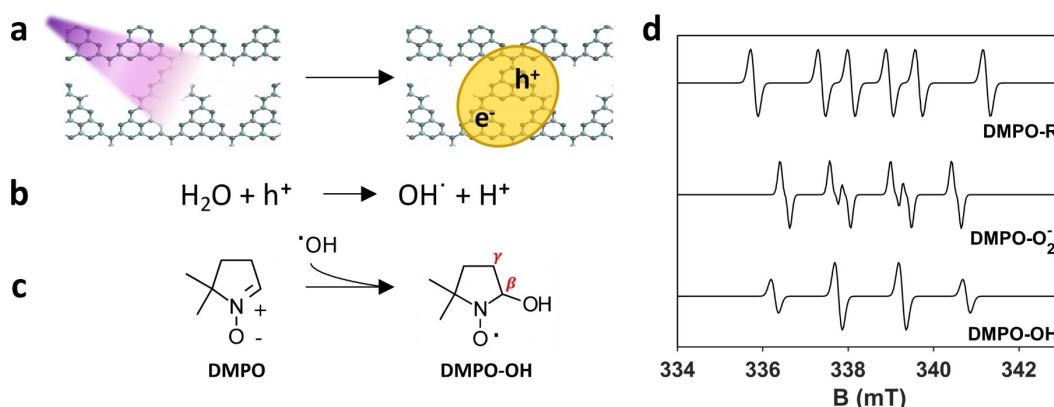
ChemPhotoChem

Review
doi.org/10.1002/cptc.202300203

Chemistry Europe
European Chemical
Societies Publishing

Figure 6. a) photoexcitation of carbon nitride and formation of an electron/hole pair. b) example of a redox process (oxidation of water) responsible for the formation of short-lived primary and reactive radical (OH$^{\bullet}$). c) Reaction between DMPO spin adduct with a OH$^{\bullet}$ radical. The position of the β and γ protons are labelled in red. d) Simulated EPR spectra form DMPO spin adducts with hyperfine couplings reported in Table 4.

4.7. Spin trapping

The detection of well-resolved hyperfine coupling is at the basis of the identification of short-lived reactive oxygen species (ROS) generated at the solid-liquid interface by light-excitation of CN (or any photocatalyst[67]) and subsequent electron/hole transfer to solvent or substrate molecules. In the most general scheme, the photogenerated radical add to a spin trap (most often nitrones) to produce a stable (nitrosyl) adduct. The hyperfine values of the adducts are a fingerprint for the photogenerated radical. The most widely employed nitrone spin trap in photocatalysis research is DMPO (5,5-dimethyl-1-pyrrolyne N-oxide) that reacts with a generic radical according to the scheme reported in Figure 6. The main features of the EPR spectrum of a DMPO spin adduct are the hyperfine coupling constants due to ^{14}N ($I=1$) and to ^{1}H ($I=1/2$) in position 2 (H$_{\beta}$) and both are sensitive to the nature of the incoming radical (Figure 6c). In some cases, notably DMPO-O$_2^-$, the hyperfine coupling with a proton in γ is also detectable. Therefore, the EPR spectrum of the DMPO adduct can be used to unravel the nature of the radical and for quantitative evaluations of the radical concentration. The g-value of the adducts usually falls in the range 2.005–2007 but varies depending on the trapped radical. However, the experimental spectra should also be accompanied by simulation and comparison with previous literature data,[38] see for instance the online NIEHS database.[68] Table 4 provides hyperfine parameters typical of the most common spin adduct formed by DMPO.

Spin-trapping is simple and effective, however, its proper use requires to be aware of all the experimental parameters discussed in the previous sections (e.g. microwave power), but also of specific subtleties intrinsic to the method. In particular, considered that only spin-adducts and not primary radicals are detected, the lifetime and trapping efficiency of each adduct should be assessed when multiple radicals are formed and quantification (absolute or relative) is attempted. Moreover, thorough cross-checking and control experiments are mandatory to avoid fallacious assignment of the detected signals which may be due to side-reactions. For instance, the spin-trap itself may be prone to photo-degradation under intense light yielding paramagnetic by-products that could be mistaken for genuine catalytic intermediates or it is widely known that the DMPO-O$_2^-$ adduct converts to DMPO-OH over time.

4.8. Guideline for reporting EPR data

Since most EPR signals of carbon nitride are simple unresolved lines, it is fundamental to report them in the most consistent way in order to allow for meaningful comparisons and avoid over or misinterpretation. In the following we provide a check list that we believe will prove useful:

1. Always clearly state the type of carbon nitride material the EPR data refer to;
2. Report the experimental g-value(s) with the highest number of significant digits compatible with the working microwave frequency and the field calibration standard used;
3. Report the measured signal width at least as the peak-to-peak separation;
4. Simulate the experimental data to ascertain if the line is Lorentzian (no inhomogeneous broadening), Gaussian (inhomogeneous broadening due to unresolved hyperfine coupling) or Voigt (admixture of Lorentzian and Gaussian lines);
5. Quantify the number of spin from the double integral, bearing in mind (and accounting for) the errors due to the baseline correction. Quantification from peak-to-peak line

Table 4. Representative hyperfine couplings for DMPO spin adducts. Note that the values may vary depending on the experimental conditions (e.g. solvent polarity, pH).

Spin adduct	^{14}N a_{iso} (MHz)	^{1}H$_{\beta}$ a_{iso} (MHz)	^{1}H$_{\gamma}$ a_{iso} (MHz)
DMPO-OH	42.0	42.0	–
DMPO-O$_2^-$	40.0	32.7	3.3
DMPO-alkyl	44.5	63.8	–

ChemPhotoChem

Review
doi.org/10.1002/cptc.202300203

Chemistry Europe
European Chemical
Societies Publishing

intensity is meaningful only if a single type of paramagnetic centre is present;

6. When employing light excitation, always state the wavelength employed, the irradiation time and the photon flux, or at least the optical power at the source. If a pulsed laser is used the energy-per-pulse should be quoted;

7. Spin trapping experiments should always be accompanied by listing of the experimental conditions (pH, solvent/buffer, …) spectral simulation and thorough validation.

These simple guidelines produce awareness of best practices and foster an informed use of EPR spectroscopy in CN research.

5. How can EPR contribute to the understanding of carbon nitride photophysics and photochemistry?

While optical spectroscopy provides a general view of the light-matter interaction in CN, EPR selectively informs on the population of defective states that are implicate in the (photo)chemical reactivity of the material.

To obtain the most from the technique, EPR should always be interpreted and planned in light of optical spectroscopy data. This is because EPR measurements can be conducted under different configuration that we summarise here.

– The formation and population of intra-bandgap state associated with defective species can be probed by light-induced EPR. The experiment can be conducted under broadband or monochromatic irradiation and comparison can provide insightful information. For instance, monochromatic irradiation below and above the bandgap can be used to prove the existence of empty and doubly occupied states;

– The chemical reactivity under photo-irradiation can be followed by measuring the EPR signal in the presence of a reactant (e.g. adsorbate, spin-trap);

– The formation of short-lived paramagnetic species (e.g. triplet states and charge carriers) can be ascertained by time-resolved EPR (TR-EPR) employing pulsed light excitation.[13] While in the standard light-induced EPR approach one observes a steady state population, TR-EPR allows the detection of transient species. This is a more sophisticated experiment not widely available but that holds great promises in defining the photophysics and photochemistry of CN.

Figure 7, reports a Jablonski diagram that summarizes the paramagnetic species relevant to the photophysis of CN. A thorough quantitative understanding of the diagram in Figure 7 - which entails the definition of all states involved, their lifetimes and transition rates - is a considerable undertaking that will definitely benefit of the synergic interplay between optical and EPR spectroscopy. This is because optical spectroscopy has a very high time resolution and is able to detect most species formed upon photoexcitation. On the other hand, EPR spectroscopy, although with lower time resolution, is able to unequivocally identify and quantify paramagnetic species by
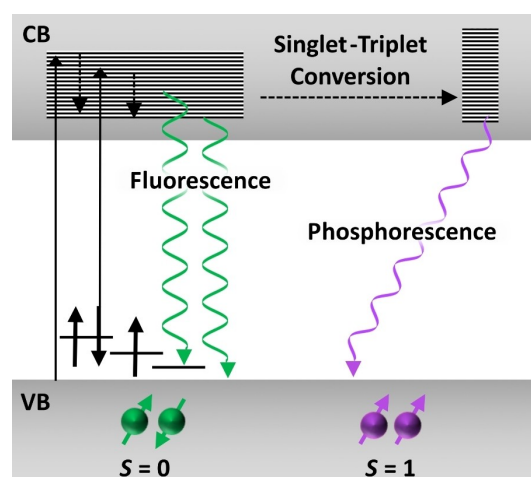

Figure 7. Schematic Jablonski diagram of the states determining the photophysics of CN. Singly occupied intragap defective states are responsible for the EPR signal in dark conditions, while doubly occupied and empty states can trap photogenerated holes and electrons.

their spin quantum number providing constraints to interpret complex optical data.[13]

The combined magneto-optical approach has been key to the understanding the complex mechanism of photosynthesis and, more recently, organic photovoltaics. Therefore, we believe it holds great promise also in the case of a complex photo-active materials such as carbon nitride.

6. Conclusions

We hope this review showcases the potentialities of EPR spectroscopy in CN research. We do believe that the information derived from different EPR techniques are numerous and can be successfully integrated to gain a comprehensive description on the photophysics of native and photo-generated radicals as well as of their local and extended structures.

We note however that, when possible, it is always beneficial to complement and integrate EPR with optical spectroscopy data. This is because the methods are sensitive to different species but also span different time-scales. A synergic approach is bound to yield the most comprehensive framework to understand the complex photophysics and photochemistry of CN and other polycrystalline inorganic semiconductors.

7. Contributor Roles

A.A.: Data curation; Visualization; Writing – original draft. P.F.: Writing – review & editing. M.C.: Writing – review & editing. E.S.: Conceptualization; Supervision; Project administration; Writing – review & editing

Acknowledgements

Conflict of Interests

The authors declare no conflict of interest.

Data Availability Statement

Data sharing is not applicable to this article as no new data were created or analyzed in this study.

[1] S. Cao, J. Low, J. Yu, M. Jaroniec, *Adv. Mater.* **2015**, *27* (13), 2150–2176.
[2] G. Algara-Siller, N. Severin, S. Y. Chong, T. Björkman, R. G. Palgrave, A. Laybourn, M. Antonietti, Y. Z. Khimyak, A. V. Krasheninnikov, J. P. Rabe, U. Kaiser, A. I. Cooper, A. Thomas, M. J. Bojdys, *Angew. Chem. Int. Ed.* **2014**, *53* (29), 7450–7455.
[3] S. Mazzanti, A. Savateev, *ChemPlusChem* **2020**, *85*, 2499–2517.
[4] M. Melchionna, P. Fornasiero, *ACS Catal.* **2020**, *10*, 5493–5501.
[5] Y. Wang, J. S. Zhang, X. C. Wang, M. Antonietti, H. R. Li, *Angew. Chem. Int. Ed.* **2010**, *49*, 3356–3359.
[6] S. Yang, Y. Gong, J. Zhang, L. Zhan, L. Ma, Z. Fang, R. Vajtai, X. Wang, P. M. Ajayan, *Adv. Mater.* **2013**, *25*, 2452–2456.
[7] K. L. Corp, C. W. Schlenker, *J. Am. Chem. Soc.* **2017**, *139*, 7904–7912.
[8] V. W. Lau, I. Moudrakovski, T. Botari, S. Weinberger, M. B. Mesch, V. Duppel, J. Senker, V. Blum, B. V. Lotsch, *Nat. Commun.* **2016**, *7*, 12165.
[9] V. W. Lau, V. W. Yu, F. Ehrat, T. Botari, I. Moudrakovski, T. Simon, V. Duppel, E. Medina, J. K. Stolarczyk, J. Feldmann, V. Blum, B. V. Lotsch, *Adv. Energy Mater.* **2017**, *7*, 1602251.
[10] Y. Chen, B. Wang, S. Lin, Y. Zhang, X. Wang, *J. Phys. Chem. C* **2014**, *118*, 29981–29989.
[11] F. Longobardo, G. Gentile, A. Criado, A. Actis, S. Colussi, V. Dal Santo, M. Chiesa, G. Filippini, P. Fornasiero, M. Prato, M. Melchionna, *Mater. Chem. Front.* **2021**, *5*, 7267–7275.
[12] K. Takanabe, *ACS Catal.* **2017**, *7* (11), 8006–8022.
[13] A. Actis, M. Melchionna, G. Filippini, P. Fornasiero, M. Prato, M. Chiesa, E. Salvadori, *Angew. Chem. Int. Ed.* **2023**, *62* (48), e202313540.
[14] G. Wolfowicz, F. J. Heremans, C. P. Anderson, S. Kanai, H. Seo, A. Gali, G. Galli, D. D. Awschalom, *Nat. Rev. Mater.* **2021**, *6*, 906–925.
[15] W. R. Scheidt, C. A. Reed, *Chem. Rev.* **1981**, *81*, 543–555.
[16] I. A. Gural'skiy, S. I. Shylin, V. Ksenofontov, W. Tremel, *Eur. J. Inorg. Chem.* **2017**, *24*, 3125–3131.
[17] C. Nitu, S. Crespi, *J. Phys. Org. Chem.* **2023**, *36*, 1.
[18] N. Hoffmann, *J. Phys. Org. Chem.* **2015**, *28* (2), 121–136.
[19] M. Chiesa, S. Livraghi, M. C. Paganini, E. Salvadori, E. Giamello, *Chem. Sci.* **2020**, *11*, 6623–6641.
[20] F. Fina, S. K. Callear, G. M. Carins, J. T. S. Irvine, *Chem. Mater.* **2015**, *27* (7), 2612–2618.
[21] *Electron Paramagnetic Resonance-A Practitioners Toolkit*, (Eds. M. Brustolon, E. Giamello), John Wiley & Sons, **2009**.
[22] M. M. Roessler, E. Salvadori, *Chem. Soc. Rev.* **2018**, *47*, 2534.
[23] Z. Barbieriková, D. Dvoranová, V. Brezová in *Materials Science in Photocatalysis*, Eds. E. I. García-López, L. Palmisano, Elsevier, **2021**.
[24] R. J. Gambino, J. A. Thompson, *Solid State Commun.* **1980**, *34*, 15–18.
[25] J. R. C. Barklie, *Diamond Relat. Mater.* **2001**, *10*, 174.
[26] D. J. Miller, D. R. McKenzie, *Thin Solid Films* **1983**, *108* (3), 257–264.
[27] J. González-Hernández, R. Asomoza, A. Rayes-Mena, *Solid State Commun.* **1988**, *67* (11), 1085–1088.
[28] E. G. Gerstner, P. Lukins, D. R. McKenzie, D. G. McCulloch, *Phys. Rev. B* **1996**, *54*, 14504.
[29] M. Fanciulli, G. Fusco, A. Tagliaferro, *Diam. Relat. Mater.* **1997**, *6* (5), 725–729.
[30] M. M. Golzan, D. R. McKenzie, D. J. Miller, S. J. Collocott, G. A. J. Amaratunga, *Diam. Relat. Mater.* **1995**, *4* (7), 912–916.
[31] F. Tampieri, S. Silvestrini, R. Riccò, M. Maggini, A. Barbon, *J. Mater. Chem. C* **2014**, *2*, 8105.
[32] S. S. Rao, A. Stesmans, Y. Wang, Y. Chen, *Physica E Low Dimens. Syst. Nanostruct.* **2012**, *44* (6), 1036–1039.
[33] B. Wang, A. J. Fielding, R. A. W. Dryfe, *ACS Appl. Nano Mater.* **2019**, *2*, 19–27.
[34] B. Wang, A. J. Fielding, R. A. W. Dryfe, *J. Phys. Chem. C* **2019**, *123* (36), 22556–22563.
[35] F. Gerson, W. Huber, *Electron Spin Resonance Spectroscopy of Organic Radicals*, Wiley-VCH Verlag GmbH & Co., **2003**, Chapter 6, pp. 100–102.
[36] W. Gordy, *Theory and Applications of Electron Spin Resonance*, John Wiley & Sons, Inc., **1980**, table 9.7, p. 504.
[37] G. R. Eaton, S. S. Eaton, D. P. Barr, R. T. Weber, *Quantitative EPR*, SpringerWienNewYork, **2010**.
[38] D. Dvoranová, Z. Barbieriková, M. Mazúr, E. I. Garcia-Lopez, G. Marcì, K. Lušpai, V. Brezová *J. Photochem. Photobiol. A* **2019**, *375*, 100–113.
[39] A. Actis, M. Melchionna, G. Filippini, P. Fornasiero, M. Prato, E. Salvadori, M. Chiesa, *Angew. Chem. Int. Ed.* **2022**, *61* (43), e202210640.
[40] M. Lacerda, M. Lejeune, B. J. Jones, R. C. Barklie, R. Bouzerar, K. Zellama, N. M. J. Conway, C. Godet, *J. Non-Cryst. Solids* **2002**, *299*, 907.
[41] M. Tabbal, T. Christidis, S. Isber, P. Merel, M. A. El Khakani, M. Chaker, A. Amassian, L. Martinu, *J. Appl. Phys.* **2005**, *98*, 044310.
[42] J. S. Zhang, G. G. Zhang, X. F. Chen, S. Lin, L. Mohlmann, G. Dolega, G. Lipner, M. Antonietti, S. Blechert, X. C. Wang, *Angew. Chem. Int. Ed.* **2012**, *51*, 3183–3187.
[43] T. Suter, V. Brázdová, K. McColl, T. S. Miller, H. Nagashima, E. Salvadori, A. Sella, C. A. Howard, C. W. M. Kay, F. Corà, P. F. McMillan, *J. Phys. Chem. C* **2018**, *122*, 25183–25194.
[44] D. Rovnyak, M. Baldus, B. A. Itin, M. Bennati, A. Stevens, R. G. Griffin, *J. Phys. Chem. B* **2000**, *104*, 9817–9822.
[45] V. W. Lau, D. Klose, H. Kasap, F. Podjaski, M. C. Pignie, E. Reisner, G. Jeschke, B. V. Lotsch, *Angew. Chem. Int. Ed.* **2017**, *56*, 510–514; *Angew. Chem.* **2017**, *129*, 525–529.
[46] G. Fanchini, S. C. Ray, A. Tagliaferro, E. Laurenti, *Diamond Relat. Mater.* **2002**, *11*, 1143.
[47] V. W. Lau, B. V. Lotsch, *Adv. Energy Mater.* **2022**, *12*, 2101078.
[48] D. Dvoranová, M. Mazúr, I. Papailias, T. Giannakopoulou, C. Trapalis, V. Brezová, *Catalysts* **2018**, *8*, 47.
[49] M. Caux, F. Fina, J. T. S. Irvine, H. Idriss, R. Howe, *Catal. Today* **2017**, *287*, 182–188.
[50] J. S. Zhang, G. G. Zhang, X. Chen, S. Lin, L. Möhlmann, G. Dołęga, G. Lipner, M. Antonietti, S. Blechert, X. C. Wang, *Angew. Chem., Int. Ed.* **2012**, *51*, 13, 3183–3187.
[51] D. Hollmann, M. Karnahl, S. Tschierlei, K. Kailasam, M. Schneider, J. Radnik, K. Grabow, U. Bentrup, H. Junge, M. Beller, S. Lochbrunner, A. Thomas, A. Brückner, *Chem. Mater.* **2014**, *26*, 1727.
[52] W. Ho, Z. Zhang, M. Xu, X. Zhang, X. Wang, Y. Huang, *Appl. Catal. B* **2015**, *179*, 106–112.
[53] A. Barbon, M. Brustolon, *Appl. Magn. Reson.* **2012**, *42*, 197–210.
[54] N. Huda, J. A. Turner, *J. Appl. Phys.* **2010**, *107*, 1237032010.
[55] S. Van Doorslaer, *EPR Spectroscopy: Fundamentals and Methods*, (Eds.: D. Goldfarb, S. Stoll), eMagRes, Wiley, **2018**, pp. 377–400.
[56] J. R. Harmer, *EPR Spectroscopy: Fundamentals and Methods*, (Eds.: D. Goldfarb, S. Stoll), eMagRes, Wiley, **2018**, pp. 331–358.
[57] E. Salvadori, M. Chiesa, A. Buonerba, A. Grassi, *Chem. Sci.* **2020**, *11*, 12436.
[58] A. Actis, E. Salvadori, M. Chiesa, *Catal. Sci. Technol.* **2021**, *11*, 5191.
[59] P. C. Bruzzese, E. Salvadori, B. Civalleri, S. Jäger, M. Hartmann, A. Pöppl, M. Chiesa, *J. Am. Chem. Soc.* **2022**, *144* (29), 13079–13083.
[60] E. Raciti, S. Manoj Gali, M. Melchionna, G. Filippini, A. Actis, M. Chiesa, P. Fornasiero, M. Prato, D. Beljonne, R. Lazzaroni, *Chem. Sci.* **2022**, *13*, 9927–9939.
[61] G. Filippini, F. Longobardo, L. Forster, A. Criado, G. Di Carmine, L. Nasi, C. D'Agostino, M. Melchionna, P. Fornasiero, M. Prato, *Sci. Adv.* **2020**, *6*, eabc9923.
[62] J. Wang, D. Hao, J. Ye, N. Umezawa, *Chem. Mater.* **2017**, *29* (7), 2694–2707.
[63] G. Di Liberto, S. Tosoni, G. Pacchioni, *Catal. Sci. Technol.* **2021**, *11*, 3589–3598.

ChemPhotoChem

Review
doi.org/10.1002/cptc.202300203

Chemistry Europe
European Chemical
Societies Publishing

[64] G. Jeschke, *EPR Spectroscopy: Fundamentalsand Methods*, (Eds.: D. Goldfarb, S. Stoll), eMagRes, Wiley, **2018**, pp. 401–424.

[65] P. P. Borbat, J. H. Freed, *EPR Spectroscopy: Fundamentalsand Methods*, (Eds.: D. Goldfarb, S. Stoll), eMagRes, Wiley, **2018**, pp. 425–462.

[66] E. Salvadori, E. Fusco, M. Chiesa, *J. Phys. Chem. Lett.* **2022**, *13* (5), 1283–1289.

[67] M. Chiesa, E. Giamello, S. Livraghi, M. C. Paganini, V. Polliotto, E. Salvadori, *J. Phys. Condens. Matter* **2019**, *31*, 444001.

[68] https://tools.niehs.nih.gov/stdb/index.cfm/spintrap/.